Global and Planetary Change 110 (2013) 223–235

Contents lists available at ScienceDirect

Global and Planetary Change

journal homepage: www.elsevier.com/locate/gloplacha

Modern sedimentation and morphology of the subaqueous Mekong Delta, Southern Vietnam

Daniel Unverricht [a,*], Witold Szczuciński [b], Karl Stattegger [a], Robert Jagodziński [b], Xuan Thuyen Le [c], Laval Liong Wee Kwong [d]

[a] Institute of Geosciences - Department of Sedimentology, Christian-Albrechts-University of Kiel, Germany
[b] Institute of Geology, Adam Mickiewicz University, Poznań, Poland
[c] Institute of Resources Geography, VAST, Ho Chi Minh City,Vietnam
[d] Environment Laboratories, International Atomic Energy Agency, 4 Quai Antoine 1er, MC 98000, Monaco

ARTICLE INFO

Article history:
Received 28 April 2011
Revised 25 August 2012
Accepted 14 December 2012
Available online 14 January 2013

Keywords:
Mekong Delta
sedimentation
grain size distribution
subaqueous delta morphology
sediment accumulation rate

ABSTRACT

The Mekong River Delta is among the Asian mega-deltas and is influenced by various factors including tides (meso-tidal system), waves, coastal currents, monsoon-driven river discharge and human impact (agriculture, fishing, sand dredging, tourism). The present study aims to document the seafloor relief, sediment distribution and sediment accumulation rates to interpret modern sediment transport directions and main sedimentation processes in the subaqueous Mekong Delta. The major results of this investigation include the detection of two delta fronts 200 km apart, one at the mouth of the Bassac River (the biggest branch of the Mekong Delta) and the other around Cape Ca Mau (most south-western end of the Mekong Delta). Additionally, a large channel system runs in the subaqueous delta platform parallel to the shore and between the two fronts. The sediment accumulation rates vary greatly according to the location in the subaqueous delta and have reached up to 10 cm/yr for the last century. A cluster analysis of surface sediment samples revealed two different sediment types within the delta including a well-sorted sandy sediment and a poorly sorted, silty sediment. In addition, a third end member with medium to coarse sand characterised the distant parts of the delta at the transition to the open shelf. The increase of organic matter and carbonate content to the bottom set area and other sedimentary features such as shell fragments, foraminiferas and concretions of palaeo-soils that do not occur in delta sediments, supported grain size-based classification. Beginning in front of the Bassac River mouth, sedimentary pattern indicates clockwise sediment transport alongshore in the western direction to a broad topset area and the delta front around Cape Ca Mau. Our results clearly show the large lateral variability of the subaqueous Mekong Delta that is further complicated by strong monsoon-driven seasonality. River, tidal and wave forcing vary at local and seasonal scales with sedimentary response to localised short-term depositional patterns that are often not preserved in long-term geological records.

1. Introduction

The ongoing natural and human-driven global changes result in important variations in the sediment flux from land to ocean (Syvitski et al., 2005), which are perceptible in the coastal zone and particularly in river deltas (Syvitski and Saito, 2007; Syvitski et al., 2009). The recent reduction of sediment input due to river damming and the resulting coastal erosion impacted the coastal zone (Milliman and Ren, 1995). Ranked among the 10 largest suppliers of sediments to the world's oceans (Milliman and Meade, 1983), and with estimated sediment discharge of 160 million tonnes per year (Milliman and Ren, 1995), the sediment discharge of Mekong River may diminish due to existing dams (Kummu et al., 2010; Wang et al., 2011). Large river systems complicate the comparison of the sediment flux estimates with the actual fluxes in the coastal zone because the final destination of the river sediments and the dominating sedimentary processes remain little understood.

A recent attempt to combine data from various river systems explored the driving processes on the dispersal and accumulation of riverine sediments in the coastal zone and defined the following important criteria: sediment discharge, shelf width, and wave and tidal conditions (Walsh and Nittrouer, 2009). Many more factors may affect the delta, however, including processes acting in the river catchment, the coastal zone and the marine realm (Vörösmarty et al., 2003; Kummu and Varis, 2007; Syvitski and Saito, 2007; Kummu et al., 2010; Yang et al., 2011). In many cases, lacks of good spatial and temporal data coverage limit these discussions. Similarly, in the Mekong River Delta, the sediment depocenter in a subaqueous part of the delta was only recently

* Corresponding author at: University of Kiel, Institute of Geosciences – Sedimentology, Coastal and Continental Shelf Research, Otto-Hahn-Platz 1, 24118 Kiel, Germany. Tel.: +49 4318803469; fax: +49 4318804376.
E-mail address: unverricht@gpi.uni-kiel.de (D. Unverricht).

0921-8181/$ – see front matter © 2012 Elsevier B.V. All rights reserved.
http://dx.doi.org/10.1016/j.gloplacha.2012.12.009

documented through several seismic profiles and 6 short sediment cores (Xue et al., 2010).

The deltas also changed in the past, and understanding their developments proves valuable for predicting their future evolution. In the case of the Mekong River Delta, land-based borehole data and seismic surveys recorded the Holocene delta evolution from the initiation of delta progradation around 8.0 ka BP to the present (Nguyen et al., 2000; Ta et al., 2002b; Tamura et al., 2009; Xue et al., 2010; Proske et al., 2011; Hanebuth et al., 2012; Tamura et al., 2012). During its development, the delta character changed from tide-dominated into a wave- and tide-dominated, and its shape and the orientation of the coastline changed through time (Ta et al., 2002a). The reconstruction of delta development is based on the character and structures of the sediments interpreted as a part of the subaqueous delta, but such data have not been gathered from the modern Mekong Delta, where the hydrodynamic conditions, the position of sediment within the delta and spatial and temporal relationships may be observed.

This study documents sea floor relief, sediments and sediment accumulation rates to interpret the modern sediment dispersal pattern, sedimentation processes and rates on the subaqueous Mekong Delta. Additionally, future interpretations of the Mekong River Delta evolution will benefit from this data set.

2. Regional setting

The Mekong River originates on the Tibetan Plateau and crosses China, Myanmar, Laos, Thailand, Cambodia and Vietnam, where it flows into the South China Sea (Fig. 1). Its delta plain stretches over an area of 49,500 km^2 between Phnom Penh in the Cambodian lowlands and the southeast Vietnamese coast (Le et al., 2007). Fig. 1 depicts the main distributaries, the Bassac (Hau River) and the Mekong (Tien River), which split into the 2 branches of the Bassac and 6 of the Mekong before entering the sea. Strong seasonal climatic variations in the Mekong Delta are related to the phase of the East Asian Monsoon (Hordoir et al., 2006; Mitsuguchi et al., 2008; Xue et al., 2011). The north-eastern winter monsoon dominates from November to early March with high wind stress at the south-eastern exposed coast, and the south-western summer monsoon carries precipitation towards the Mekong Delta (Mekong River Commission, 2005, 2009; Snidvongs and Teng, 2006; ISPONRE, 2009). The annual average rainfall in southern Vietnam ranges between 1600 and 2000 mm. Wind speeds can reach 20–30 m/s under stormy conditions; however, mean annual wind velocities range between 1.5 and 3.5 m/s (Institute of Strategy and Policy on natural resources and environment (ISPONRE), 2009).

The distribution of the principal surface current system in the Southern South China Sea has been attributed to the East Asian Monsoon (Wendong et al., 1998). The maximum wind stress prevails along the south-eastern coast of the Indochina Peninsula in both monsoon seasons. In the Mekong River basin, 85% (475 billion m^3) of the water discharge occurs during the wet season (May to October), and 15% (78.8 billion m^3) in the dry season (November to April) (Snidvongs and Teng, 2006; Le et al., 2007). The Mekong River Commission provides a representative documentation of the water discharge and level for the upper Mekong Delta region. Data availability of the water discharge or tidal amplitudes is however problematic for the river mouth

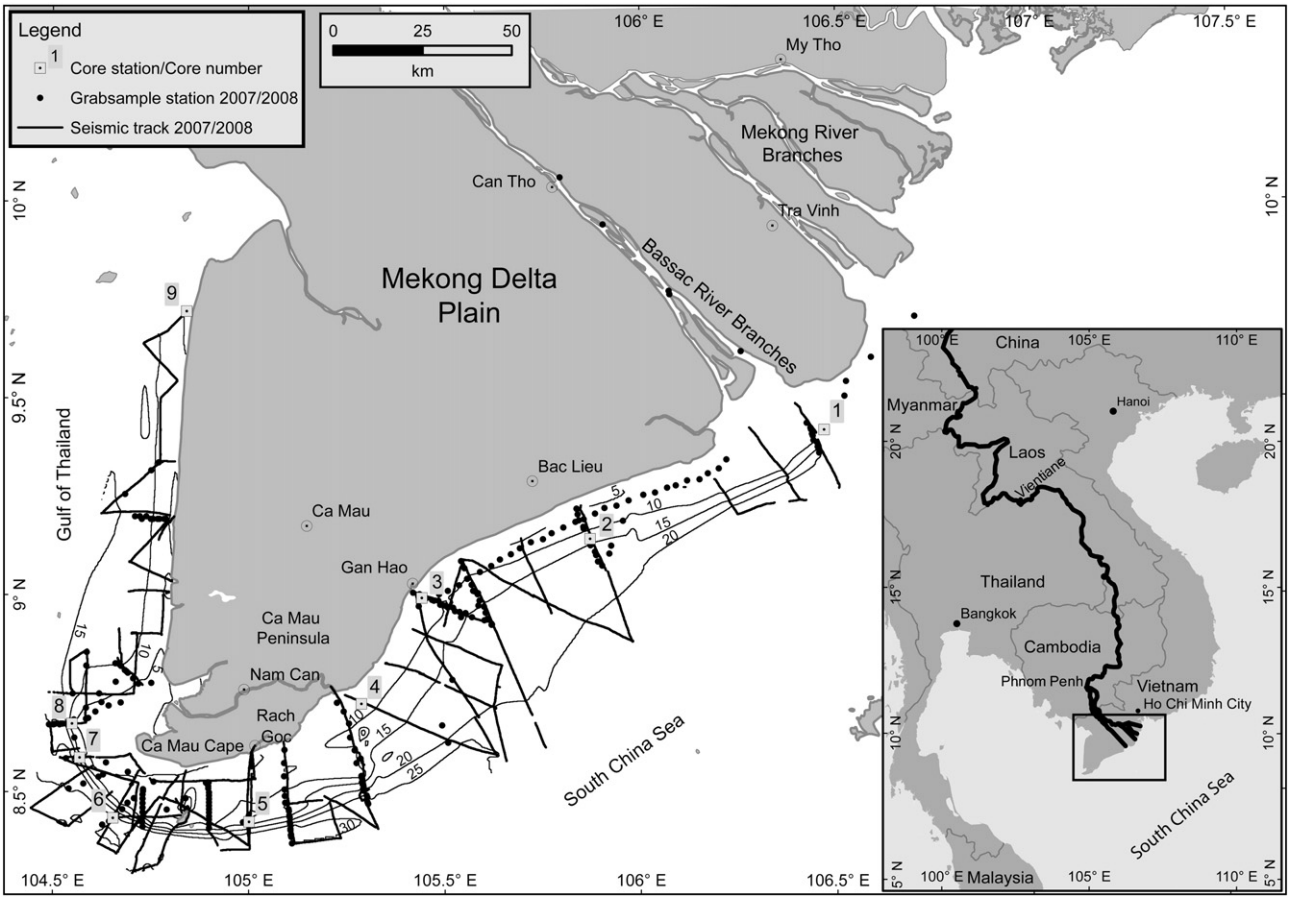

Fig. 1. The base map containing the investigated area with the subaqueous part of the Mekong Delta and adjacent continental shelf, with marked surveyed seismic lines, locations of surface sediment samples and sediment cores and the topographical features mentioned in the text. The presented bathymetry is based on own survey. The inset map shows the location of the Mekong River delta in South-east Asia.

area of all the branches. The only existing sediment load data of 160 million t/yr (Milliman and Meade, 1983) was derived before many dams were constructed. Contemporary estimates of the sedimentary retention of the existing dams along the Mekong River calculate 35–45 million t/yr in sediment (Kummu et al., 2010).

Hydrodynamics and resulting sediment-dynamics formed the asymmetric shape of the delta plain. The incoming tidal waves of the dominant M2- and K1-constituents extend from northeast to southwest via the Strait of Luzon (Fang et al., 1999; Zu et al., 2008). These waves push water masses into the coastal region and cause a meso-tidal regime in front of the Mekong Delta branches. The tidal range and regime vary along the southeast Vietnamese coast from a predominantly semi-diurnal tidal system with a mean range of 2.5–3.8 m in the east to a mixed-tide system with decreasing amplitudes towards the southwest (Nguyen et al., 2000). Diurnal tides predominate in the Gulf of Thailand with ranges of 0.5 to 1.0 m.

The sedimentary architecture of the delta plain is well investigated, especially in the region between the Mekong distributaries (Gagliano and McIntire, 1968; Nguyen et al., 2000; Ta et al., 2002b, 2005; Tamura et al., 2009, 2012; Proske et al., 2011; Hanebuth et al., 2012). The study of the subaqueous part of the Mekong Delta is far less common. Annual net southwestward transport along a mesotidal beach and respective long-term shoreline changes were observed in the Tra Vinh province in the lower Mekong Delta plain by Tamura et al. (2010). There, interseasonal surveys were carried out in the intertidal area of the Mekong Delta coast. Wave heights of 1 m in maximum were observed for this region.

Gagliano and McIntire (1968) provided first sedimentary and bathymetric results of the subaqueous Mekong Delta. Several coastal normal transects showed the subaqueous clinoform reaching more than 20 km offshore in front of the main distributaries and around Ca Mau Peninsula. Recently, seismic profiles of a higher resolution and several sediment cores revealed a Holocene subaqueous delta with up to 20 m thick sediments and a heterogeneous of topset–foreset–bottomset architecture (Xue et al., 2010). In order to refer more intensively to wide spreaded shallow subaqueous regions this article add the term of the subaqueous delta platform as a morphological description of topset areas. Further, the term delta slope is used for the foreset region.

3. Materials and methods

High-resolution seismic profiles have been recorded during two surveys (2007 and 2008) of the subaqueous Mekong Delta off Vietnam, from the Bassac River mouth to the Gulf of Thailand (Fig. 1). Using the cubic spline method, an approximated subaqueous delta shape was constructed by interpolating the seabed profiles, which were obtained from seismic surveys using the software The Kingdom Suite (Seismic Micro-Technology, U.K.). The two-way-travel-time (TWT) was converted into water depth and assigned a sound velocity of 1500 m/s, and bathymetry data were analysed in ArcGIS. However, an error of up to 1.8 m may exist between various profiles as the shown water depths could not be corrected for tides. There is no correlation to the base level or a Vietnamese tidal gauge station applied due to unknown water level variation in the subaqueous Mekong delta region, which is necessary for such a water level correction.

The surface sediments (the upper 1 cm of the seabed) of 229 stations were analysed for grain size distribution. Before the analyses, the sediments were treated with 35% H_2O_2 and sieved using a 1 mm sieve. Then, samples were analysed using the Malvern Mastersizer 2000 based on laser diffraction. The obtained results are shown in volume percentages. The grain size statistics of the obtained results were calculated using GRADISTAT software (Blott and Pye, 2001), and the grain size data were also subjected to cluster analysis with the free statistical tool R. The Centroid method and the squared Euclidean distance were used to obtain the cluster centres.

In selected surface sediment samples, the proportional masses of organic matter and carbonates were estimated using the loss on ignition method (Heiri et al., 2001; Santisteban et al., 2004). The content of organic matter results from the weight loss on ignition by 550 °C. The carbonate content (CC) was assessed from the difference in weight loss on ignition between 950 °C and 550 °C, multiplied by a factor of 1.36.

The sedimentary structures and relative changes in grain size were documented in the sediment cores using digital X-radiography images obtained from 0.6 cm thin slabs of the split core surfaces. The sediment accumulation rate (SAR) over the last few decades was assessed through the analysis of ^{210}Pb and ^{137}Cs. The ^{210}Pb activities for Cores 5 and 7 were determined using alpha spectroscopy measurements of the granddaughter nuclide ^{210}Po in the Marine Environment Laboratories of the International Atomic Energy Agency in Monaco. For these analyses, sediment samples were homogenised, spiked with a yield determinator and dissolved by acid digestion, and the ^{210}Po isotope was autoplated on a silver planchet (Flynn, 1968). Cores 6, 8 and 9 were measured using gamma spectroscopy, which allows the simultaneous measurement of ^{210}Pb and ^{137}Cs. Core 6 was measured with a high purity coaxial germanium detector (Canberra GX2520) with its remote detector chamber option (RDC-6 inches) set for low energy background reduction in the Institute of Geology at Adam Mickiewicz University in Poznań (Poland). Cores 8 and 9 were investigated at the Leibniz-Laboratory for Radiometric Dating and Isotope Research in Kiel (Germany). Samples for the gamma analyses were dried, homogenised and measured on average for approximately 150 h each.

The SAR was assessed from the decrease of excess ^{210}Pb activities with sediment depth, using the equation:

$$SAR = \lambda \times z \times [\ln \{A_0/A(z)\}]^{-1}$$

(Robbins and Edgington, 1975; McKee et al., 1983)

Where λ ($=0.0311\ yr^{-1}$) is the decay constant, z is the depth in the core (cm), A_0 is the specific activity of the excess ^{210}Pb at a particular reference horizon or the surface and $A(z)$ is the specific activity of the excess ^{210}Pb at depth z below the reference horizon. Excess (unsupported) ^{210}Pb activities were determined by subtracting the average supported activity of a given core from the total activity. If possible, the supported activities were calculated from the nearly uniform ^{210}Pb activity below the region of radioactive decay. In the case of Core 6, they were also confirmed by simultaneous measurements of ^{214}Pb, ^{214}Bi and ^{226}Ra using gamma spectrometry. The supported ^{210}Pb activity is 22.1 ± 1.6 Bq/kg and correlates with the supported ^{210}Pb activity of 1.09–1.44 dpm/g ($=18.1$–24 Bq/kg) in cores in the subaqueous Mekong delta region from Xue et al. (2010).

The SAR assessment was performed using the first occurrence of ^{137}Cs as a marker of the early 1950s, when it was first released on a large scale in the environment during atmospheric nuclear weapon tests (Robbins et al., 1978; Leslie and Hancock, 2008).

4. Results

4.1. Sea bed morphology

The subaqueous Mekong Delta area consists of 5 subareas distinguished by clinoform morphology (Fig. 2). With an approximately 27 km wide funnel-shaped river mouth, the Bassac dominates Area 1. The delta base is reached 28 km offshore in the south-eastern direction, and tidal and subtidal flats and shallow topsets, up to a depth of 6 m underwater, characterise the proximal littoral (Profile A-A' in Fig. 2). Southwest of the mouth of the Bassac River, the subaqueous delta platform spreads at least 10 km offshore. Distant from the coast, a sigmoidal delta slope rises to the southeast and reaches the delta base at a depth of 24 m underwater (Fig. 2). The

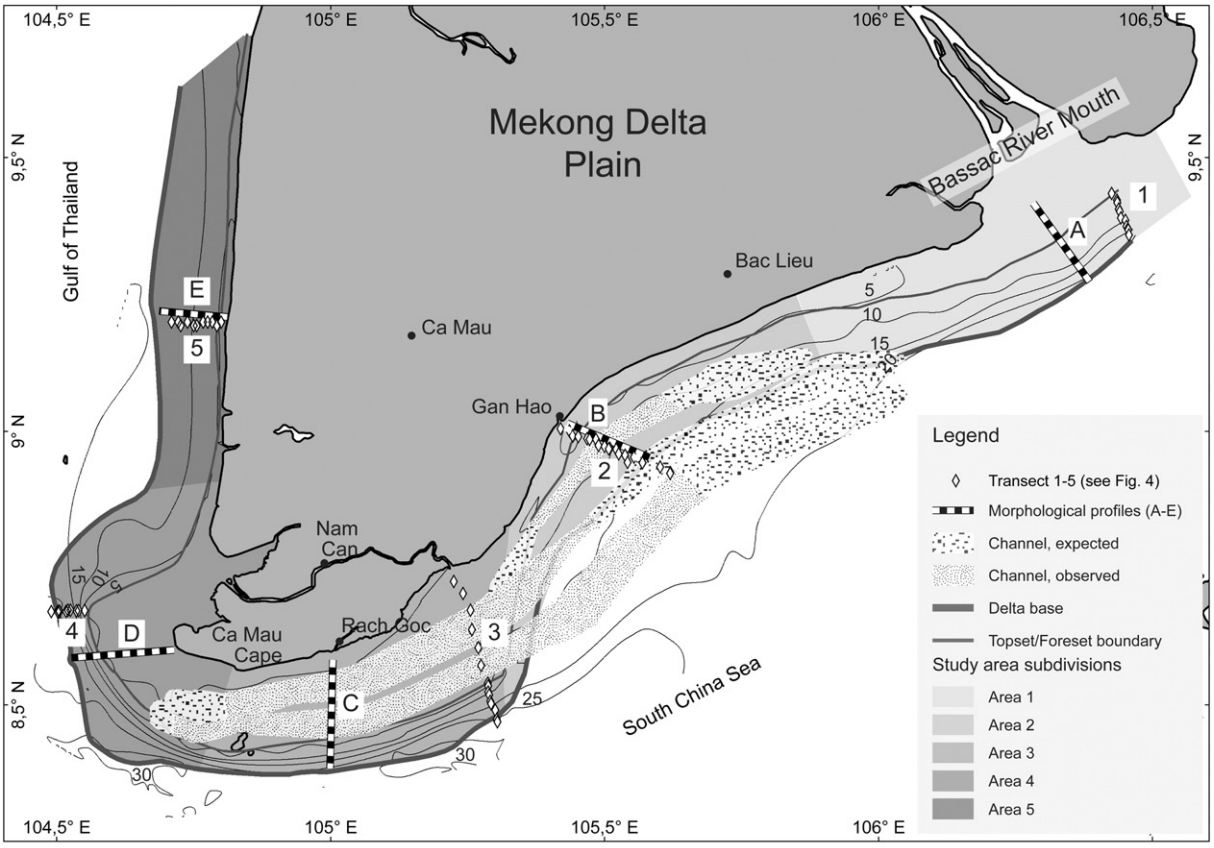

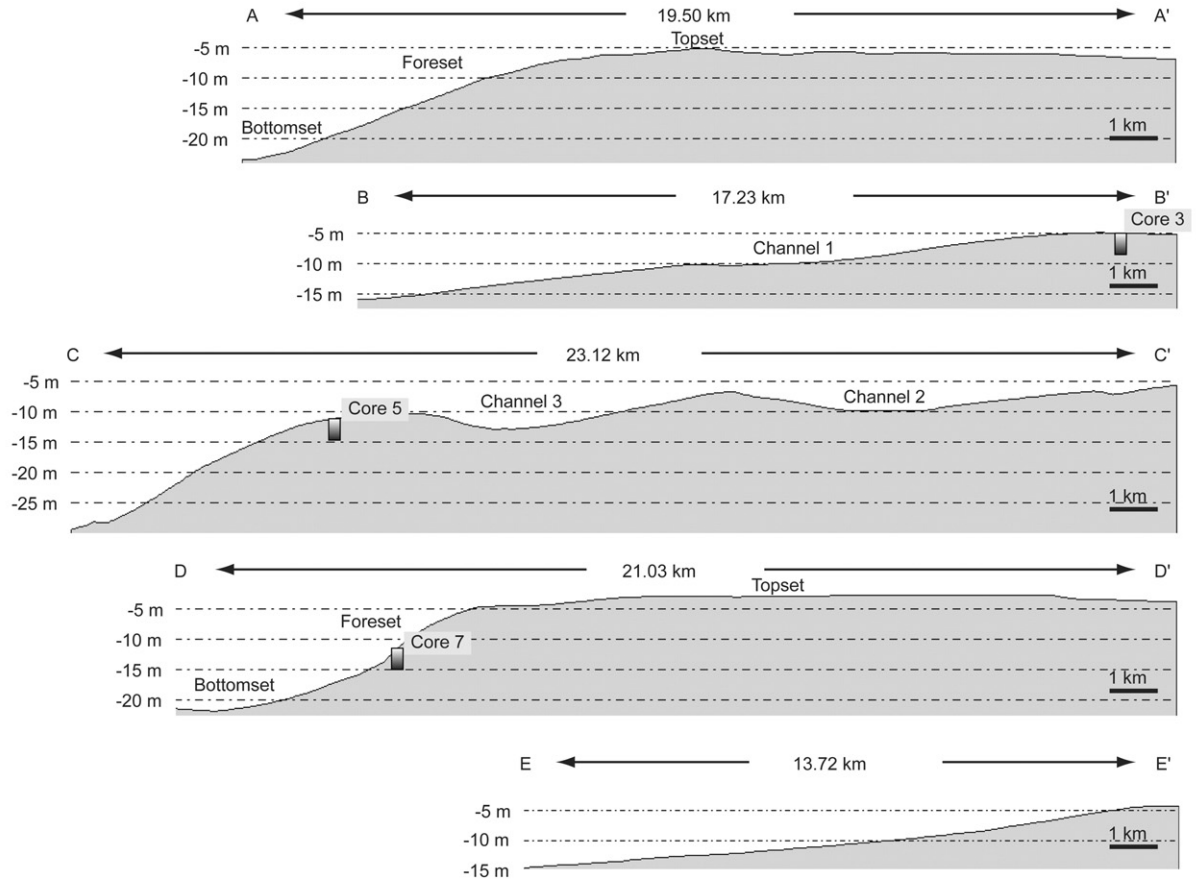

Fig. 2. Morphology of the subaqueous part of the Mekong River delta with the delta extension (delta base line), major morphological features (the break in the delta slope — topset/foreset boundary, channels), locations of morphological Profiles A to E presented below, sample transects 1–5 and the subdivision of the delta into 5 areas marked as discussed in the text. The location of sediment cores and major morphological features are marked on the morphological profiles.

slope lengths average 8 km by a mean slope angle $\alpha_{mean} = 0.05°$ ($\alpha_{max} = 0.2°$).

The width of the subaqueous delta platform in Area 2 decreases to 3.5 km in the offshore direction (Profile B-B', Fig. 2). The average slope angles reach inclinations of $\alpha_{mean} = 0.052°$ ($\alpha_{max} = 0.12°$). The most recent delta slope ends at a depth of approximately 15 m (Fig. 2). Its significant undulated shape indicates the beginning of a multiple channel system (Fig. 2). One smaller and two larger channels are spread out in an alignment parallel to the coast (unpublished data). The channel linkage is located in the subaqueous delta platform and the delta slope close to Area 3 (Fig. 2), and its extension is more than 120 km.

The essential difference between the previous areas and Area 3 is the widespread subaqueous delta platform of 1100 km^2, including the channel system (Fig. 2). Channel 2 changes westwards from 13.5 m to 3 m water depth, and a deeper offshore channel (Channel 3) is levelling off from 17 m to 6 m water depth to the west. The southern flank of Channel 3 forms the transition to the delta slope (Fig. 2). Slope angles are relatively steep ($\alpha_{max} = 0.48°$), with an average slope length of 5.7 km (min/max length = 3.4/8 km).

Around Cape Ca Mau (Area 4), a very shallow (less than 5 m) subaqueous delta platform is prograding 13.5 km offshore on average. The subaqueous Mekong Delta forms a further delta front here outside of the direct influence of distributaries (Fig. 2). It has an average slope gradient of $\alpha_{mean} = 0.054°$ ($\alpha_{max} = 0.43°$).

Along the western and north-western coast (Area 5), the subaqueous delta platform regresses abruptly to the coast by an average width of 1.8 km, and the delta base is reached at a depth of 15 m with an average slope width of 11.8 km (Fig. 2).

4.2. Surface sediments

4.2.1. Spatial sedimentary distribution and grain size end members

The surface sediments of the subaqueous Mekong Delta vary strongly in sorting and dominant grain size mode, but show a spatial pattern depending on the distance from the distributaries and their position in the delta clinoform. Near the Bassac River, fine sand prevails and silty sediment occurs in more distant regions (Figs. 3C and 4). Fine sediment (silt and sandy silt) primarily covers Area 2, but there is a distinct occurrence of sand and silty sand along the recent delta slope close to Transect 2 (Figs. 3C and 4). Except for an occurrence of silty sand along Transect 3 (Figs. 3C and 4), the southern subaqueous delta area (Area 3) is dominated by sandy silt. Cape Ca Mau forms a junction between sandy silt and silty sediments. The northward continuing subaqueous delta exposed to the Gulf of Thailand consists of silt (Figs. 3C and 4).

Cluster analysis was performed to generalise the sedimentary pattern and evaluate the grain size end members for different depositional subenvironments. The cluster analysis used the grain size parameters as the primary mode (Mode 1) for the prevailing grain size class at certain locations and the difference between the ninth and first deciles (D90–D10) as a measure of sorting. Together, the two parameters represent a particular depositional environment.

The cluster analysis defines three clusters as grain-size end members in the subaqueous Mekong Delta and the transitional shelf region (Fig. 3A and B). Cluster 1 represents most of the subaqueous delta sediment and exhibits poor sorting, and the primary mode has its cluster centre in medium silt (Fig. 3A). However, uni- or bimodal grain size distributions occur as well with different positions, where modes mainly in fine sand and silt prevail.

The second cluster is also a part of the delta sediment, but its primary mode cluster centre is fine sand, exhibiting good sorting. The spatial distribution of Cluster 2 shows consistence with the special subaqueous delta regions (Fig. 3B). The tendencies of coarse to fine sediment from near to distant regions is typical for a river mouth area, due to sorting by diminishing water velocity (Transect 1 in Fig. 4). Alongshore tidal and wind induced currents cause the same succession in coast parallel direction (Fig. 5). The well-sorted sands of Cluster 2 dominate the subaqueous delta platform in front of the Bassac River mouth (Fig. 3B), where strong currents occur. The sandy spots of Cluster 2 punctuate the fine sediment close to Transect 2 (Fig. 3B and C). Additionally, the sandy sediment of Cluster 2 distributes along the southern flanks of Channel 2 and 3 (Fig. 4).

Very poor sorting by a primary mode of medium sand predominates in Cluster 3, representing its differences from Clusters 1 and 2 (Fig. 3A). The delta base marks the landward border of Cluster 3 because it extends between the delta base and the open shelf region (Fig. 3B). This distribution was also observed in the sediment fraction >1 mm, except in the region close to Gan Hao (Fig. 3C). It represents a significant proxy for sediment interaction between the subaqueous delta and shelf sediment. This coarse fraction consists of shell fragments, foraminiferas and concretions, the latter of which are likely residuals of lateritic palaeosoils outcropped on the inner shelf.

A more detailed resolution of grain size distributions along the coastal normal transects provides a miscellaneous pattern in a higher resolution. Supplementary data of percentages from organic matter (OMC) and carbonate content (CC) coincide mainly with that pattern. The subaqueous delta platform in front of the Bassac River mouth, shown by Transect 1 (Fig. 4), accommodates well sorted fine sands (mode ~2.85 Phi), low organic matter (<1.74 wt.%) and carbonate content (<0.66 wt.%). With increasing water depths, OMC increases rapidly to more than 6.58 wt.%, and CC rises only slightly (<1.67 wt.%).

Transect 2 shows heterogeneous grain size features (Figs. 3C and 4), and is situated close to Gan Hao in Area 2. The shallow subaqueous delta platform consists predominately of very fine sand with low percentages of silt and clay. Fine silt prevails along the delta slope, where sand content decreases below 9.1 vol.%, but sand predominates along the deeper delta slope, with sand content between 45 and 99 vol.%. At the delta base, silt and clay content increase again, and the organic matter and carbonate concentration follow that trend, except near the delta base. A rapid increase of carbonate percentages (maximum = 6.97 wt.%) indicates the transition to the open shelf, where shell fragments are common.

The southern area is shown by Transect 3 (Figs. 3C and 4), which crosses both channels in that area. The silty regions of the subaqueous delta platform and channel troughs have high percentages of organic matter (>7.11 wt.%), but the southern channel flanks correlate with decreased OM-content (<5.08 wt.%). The sand fraction dominates there with up to 90 vol.%. Along the delta slope, silt prevails with increasing OM-content (Fig. 4). The highest carbonate content occurs with up to 16.2 wt.% at the delta base, where shell fragments in the sediment fraction >1 mm mark the transition to the open shelf.

Transect 4 extends along the delta front around Cape Ca Mau (Fig. 3), and silt and clay (content >94 vol.%) dominate this area, including a high OM-content (Figs. 3C and 4). At the delta base, medium sand dominates, and the carbonate content increases up to 7.21 wt.%, due to the occurrence of the sediment fraction >1 mm, where many concretions from palaeosoils, shell fragments and foraminiferas occur.

Represented by Transect 5, the subaqueous delta in the Gulf of Thailand shows a pattern similar to Transect 4, with high organic matter content and predominant silt percentages. However, it exhibits a lower gradient of the delta slope. Samples likely did not reach the transition of prodelta and shelf because no coarser sediment was found in the surface samples. The comparison of the last sample of transect 5 (Fig. 2) with the location of the delta base confirms that assumption.

4.2.2. Sedimentary structures

X-radiograph negatives of the upper 20 cm from selected cores, which were taken along the transition of the subaqueous delta platform and slope (topset to foreset), reveal a successive alternation of interbedded and interlaminated sands and silts (Fig. 5). Sand content is primarily decreasing with distance to the eastern main distributaries

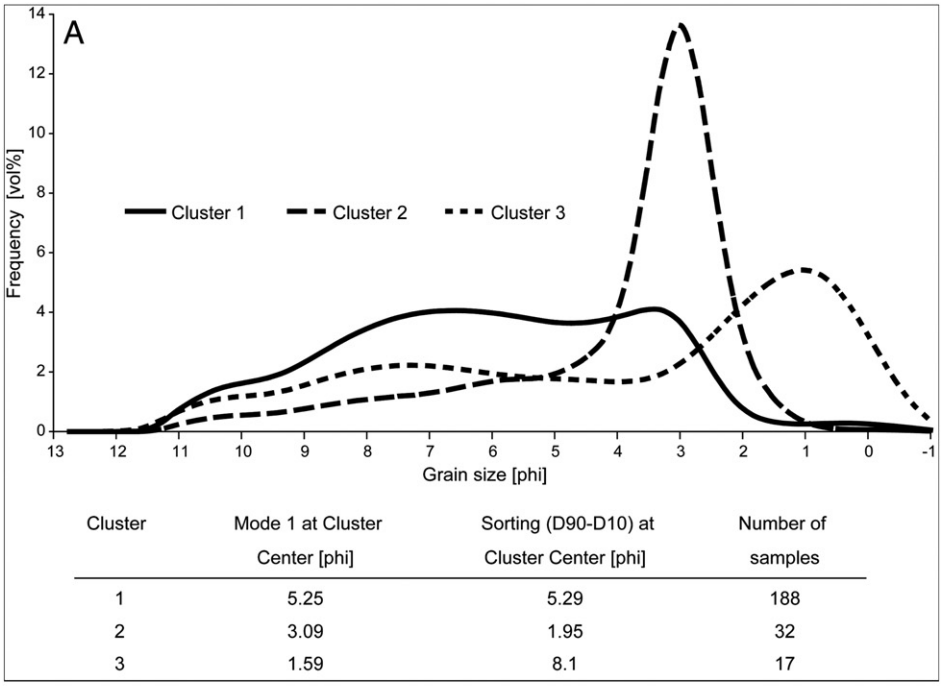

Cluster	Mode 1 at Cluster Center [phi]	Sorting (D90-D10) at Cluster Center [phi]	Number of samples
1	5.25	5.29	188
2	3.09	1.95	32
3	1.59	8.1	17

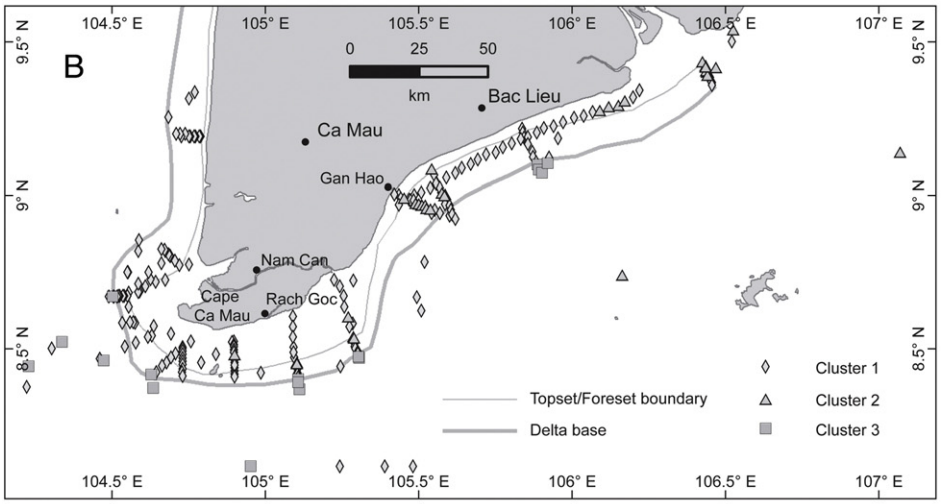

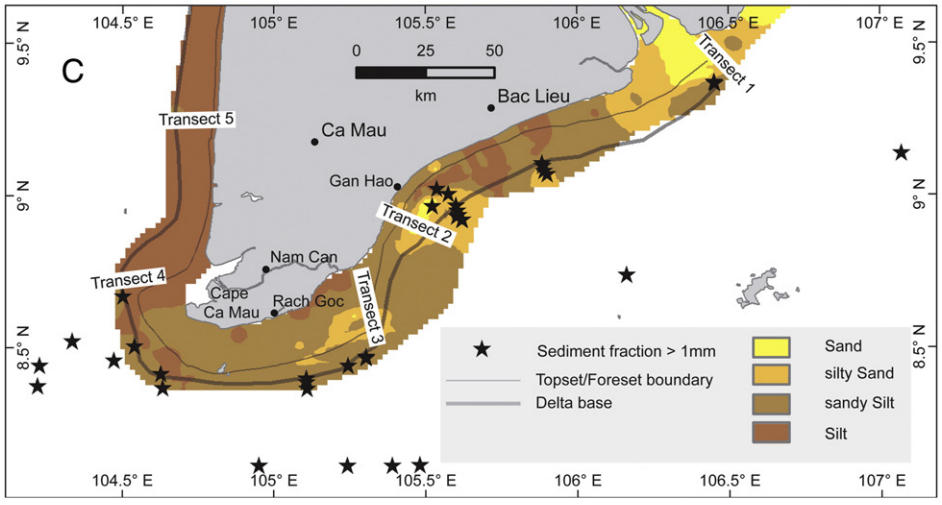

Fig. 3. A) Average grain size distributions of three sediment clusters and the numerical cluster centres (the first mode and D90-D10); B) spatial distribution of surface sediments grouped into particular clusters; C) the surface sediment map with marked surface sediments containing the fraction >1 mm.

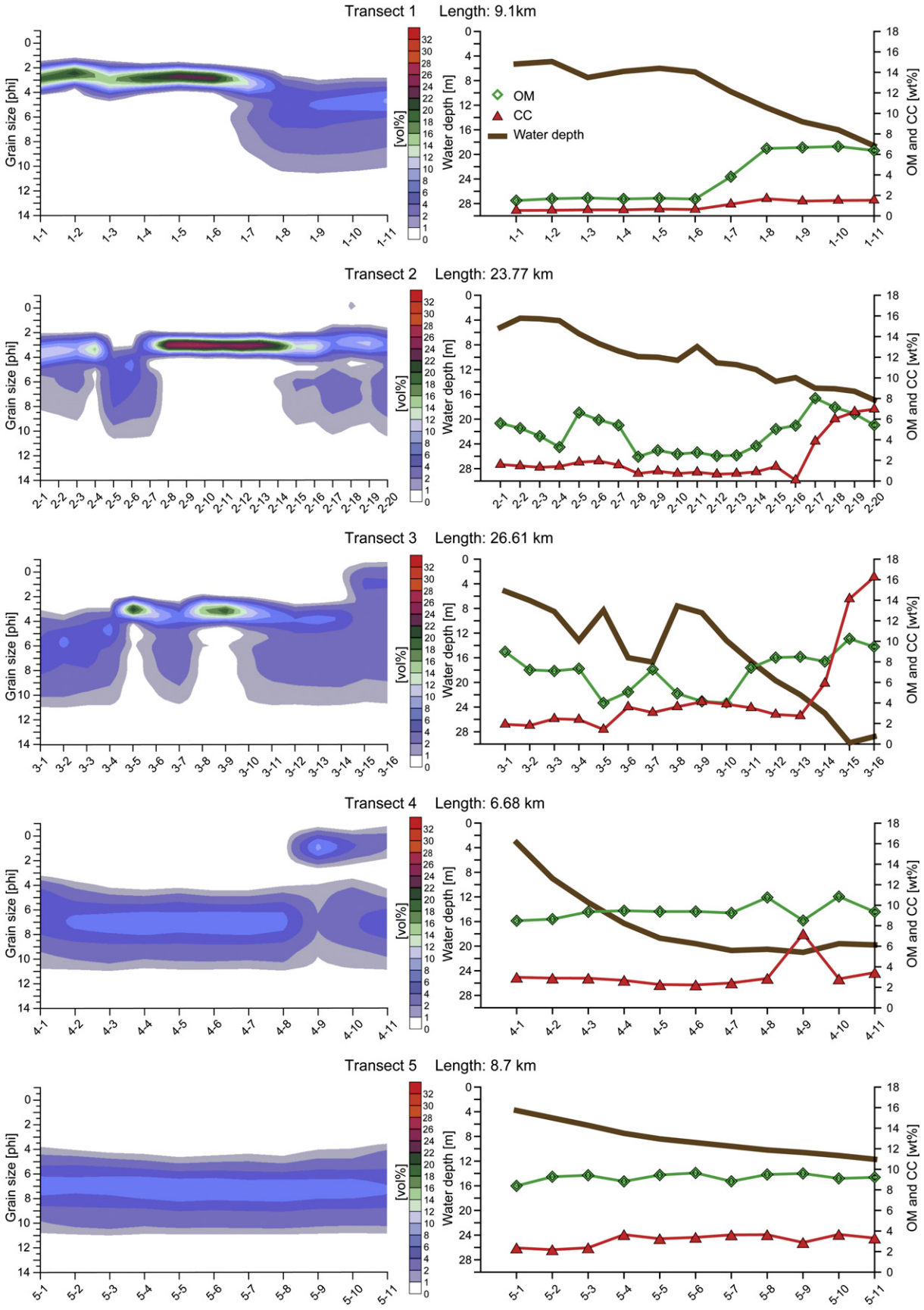

Fig. 4. Sediment properties along the five shore normal transects, grain size distribution (left hand), organic matter (OMC) and carbonate contents (CC), and seafloor morphology (right hand); see Fig. 2 for transect locations. The numbers on the x-axis refer to the sediment sampling sites along the transects.

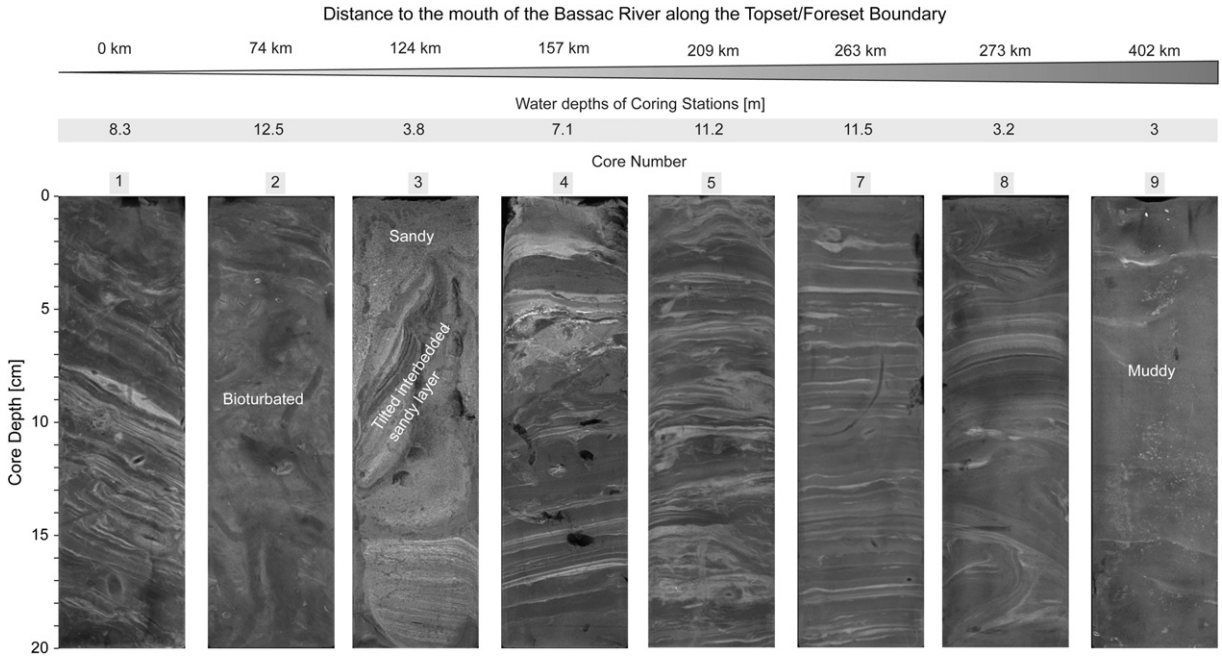

Fig. 5. X-radiograph negatives from the uppermost parts (20 cm) of eight sediment cores (see Fig. 1 for locations) aligned with increasing distance from the river mouth. The black parts in Core 4 are artefacts due to the sample preparation.

that coincide with the trend of surface sediment distribution. However, around the Gan Hao area (Fig. 1), sand dominates in the upper layers (Core 3 in Fig. 5), and X-radiograph negatives show anomalies in the sediment pattern (Core 4).

The most common sedimentary structure is lamination, which is observed in all the cores, although commonly it is disturbed. The common lamination shows changing conditions, which are probably caused due to tidal influence. Thin sandy (bright on the Fig. 5) and thicker silty laminae or layer mainly marks this lamination (darker on Fig. 5). They are horizontal (e.g. cores 5 and 7), wavy or inclined (core 1). The latter, reveals deformations and slight folding, possibly related to redeposition on the inclined sea floor. In cores dominated by mud, the thicker parts of sand laminae form loading structures, due to sinking of sand in unconsolidated mud (see for instance upper part of core 7). Some of the sandy laminae of wavy shape (e.g. core 7, Fig. 5) were likely formed as small ripple marks, and their shape is still preserved in places. Evident erosional surfaces are visible (e.g. cores 3, 4. 8), which suggest frequent redeposition of the sediments. In core 3 tilted laminations are evident (Fig. 5) which are not caused by coring, as shown in the lower horizontal layering in the core, but indicates redeposition of several centimetre in size intraclasts of sediments in form of mass movements along the delta slope. The complex sediment supply is shown by findings of shell fragments (e.g. core 4, depth 5 cm, Fig. 5), which are not representative of the delta sediment. However, it implies sediment exchange with shelf sediment, for instance during storm surges. Although the location of core 2 is relatively close to the Bassac River mouth its X-radiographs negatives reveal features of bioturbation that indicates lower deposition. In contrast, even core 9, situated far away from areas of high sediment supply, consists of fine laminated silt and clay with little traces of bioturbation, which suggest relatively high accumulation rate.

4.3. Sediment accumulation rates

Estimations of sediment accumulation rates (SARs) based on measurements of ^{137}Cs and ^{210}Pb activity (Fig. 6) use three approaches (Table 1). The first approach assumes that sediments containing ^{137}Cs have to be deposited after the early 1950s when the first atmospheric nuclear weapon tests were done. The half-life of ^{210}Pb is 22.3 yr, and no excess ^{210}Pb as a portion of the total ^{210}Pb resulting from atmospheric fallout, is expected to be detected in deposits older than a century. The second approach therefore uses the presence of excess ^{210}Pb as an indicator of sediments deposited within the last 100 yr at maximum. The third approach is based on the constant initial concentration model presented in Chapter 3. All cores indicated very high SARs. The well preserved laminations revealed unsteady sedimentation, and the measured activities are often very low. The presented calculations must therefore be treated as minimum estimates of an order of magnitude.

Core 5 is composed of laminated sandy mud (Fig. 6). The ^{210}Pb activity profile reveals a steady decrease in the activities from a depth of 22 to 102 cm. Below, the ^{210}Pb activities are almost stable, but they have not reached the supported ^{210}Pb activities. The lower activity in the uppermost sample may be due to the dilution in the larger mass of temporary deposited sediments. Assuming supported ^{210}Pb activities of about 22.1 (Bq/kg), the SAR estimations reveal a rate of slightly above 4.0 ± 2.1 cm/yr.

In Core 6, two sedimentary units are found (Fig. 6). The upper one comprises brown mud with high water content, below which there is a sharp unconformity at 200 cm core depth followed by an olive-grey and consolidated mud unit. In the lower unit, the ^{137}Cs activity is below the detection limit, and no excess ^{210}Pb activities were measured (the lower unit has higher supported ^{210}Pb activities than the upper). These sediments are at least older than 60 yr. In the upper unit, the SAR is approximately 2.6 ± 1.5 cm/yr, as calculated from the decrease in excess ^{210}Pb activities between 20 and 120 cm core depth. The upper 20 cm reveal relatively stable activities, at slightly lower rates than below, and it likely results from the dilution of temporarily deposited larger masses of sediment. The presence of ^{137}Cs in the complete upper unit suggests that the SAR could be even higher than 3.6 cm/yr.

The ^{210}Pb activity of Core 7 shows little changes. Applying supported ^{210}Pb activities from Core 6, the excess ^{210}Pb activities are found in the complete Core 7 and SAR amounts are at least 1.4 cm/yr. Very little or no change in the excess ^{210}Pb, typical for very high deposition rates and supported by the laminated sediments, suggests sediment accumulation at the rate in the order of ~10 cm/yr, or temporarily deposited during the last winter monsoon season.

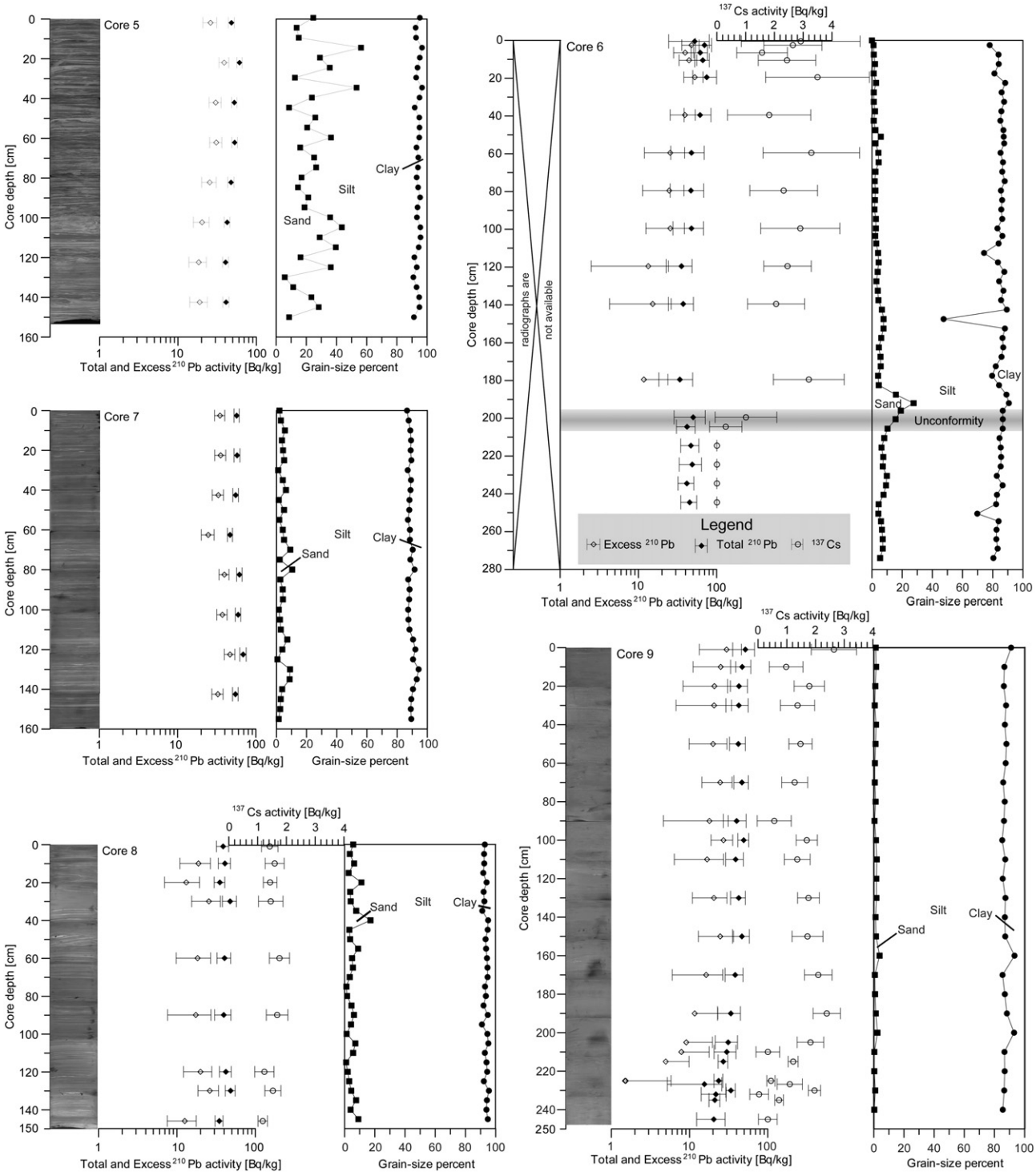

Fig. 6. X-radiographs, total and excess ^{210}Pb activities, ^{137}Cs activity and clay, silt and sand fraction percentages in the 5 cores (see Fig. 1 for locations). The ^{210}Pb activities are presented in logarithmic scale with 2-σ error. Note, there is a clear unconformity at approximately 200 cm in Core 6 separating different sediment types.

Core 8 has a very similar ^{210}Pb activity profile and estimated SAR as Core 7 (Fig. 6; Table 1). The only difference is the lower average activity. However, the sedimentary differences between the cores may cause variations in supported activities, as exemplified by the upper and lower unit in Core 6, and the SAR may be so high that the excess ^{210}Pb is diluted by the large mass of deposited sediments. The presence of ^{137}Cs throughout the core supports the very high SAR and suggests that the SAR is at least 2.5 cm/yr.

The ^{210}Pb activity profile in Core 9 is generally characterised by three parts: the uppermost 150 cm of near-uniform activities, the zone of decreasing activities down to about 225 cm and the relatively stable (supported) activities underneath these zones. The supported activities are much smaller than in the previous cores. The uppermost part has to be deposited in a very short period at a rate of more than 10 cm/yr and likely reflects the temporary (seasonal) deposition or recent rapid increase in the SAR. The calculations based on the

Table 1
Assessments of linear sediment accumulation rates (cm/yr) based on the ^{210}Pb and ^{137}Cs activity profiles (Fig. 6). Calculations are explained in the text.

Sediment accumulation rates [cm/yr]			
Core	Based on the presence of ^{137}Cs	Based on the presence of the excess ^{210}Pb	Calculated from decay of the excess of ^{210}Pb
5	–	>1	4.0±2.1
6	>3.6	>1	2.6±1.5
7	–	>1.4	>10?
8	>2.5	>1.4	>10?
9	>3.9	>2.2	>10? (upper 1.5 m); 1.6±0.4 (below 1.5 m)

decay of excess ^{210}Pb between 150 and 215 cm revealed a SAR of about 1.6±0.4 cm/yr, and the presence of ^{137}Cs in the upper 230 cm of the sediment core suggested a SAR of at least 3.9 cm/yr.

5. Discussion

Modern delta morphology and sediment dynamics are shaped mainly by waves, tides and river impact, factors that also serve as the basis for delta classification schemes the following discussion focuses on the interpretation of sedimentary processes and controlling factors in different delta regions.

5.1. Subaqueous delta division and sedimentation pattern

The results of our investigations lead to the division of the subaqueous Mekong Delta into 5 areas, instead of 4 as proposed by Xue et al. (2010). It is based on the delta morphology, sediment types and their location relative to the Bassac River, a main distributary (Table 2). Two conspicuous regions exhibit broad topsets and steep foresets and are probably the areas of the fastest delta progradation (Fig. 2, Table 2). The delta progradation takes place in two different directions (southeast and west) and in parts of the delta approximately 200 km apart: next to the river mouth and around the Ca Mau Peninsula tip (Subareas 1 and 4). These areas were already identified previously (Gagliano and McIntire, 1968; Xue et al., 2010). Our results show that the two areas differ significantly in sediment type. Fine sand dominates near the Bassac River mouth and silt and clay near Cam Mau Cape (Figs. 3C and 4). Additionally, our data set provides new information about heterogeneous sedimentary pattern due to the variable contribution of riverine and oceanographic factors (Fang et al., 1999; Nguyen et al., 2000; Zu et al., 2008).

Pronounced by narrow topsets and atypical well sorted sand along gentle, wavy foresets (Figs. 2 and 3C), Area 2 indicates in X-radiograph negatives either bioturbated laminated sand and silt or sandy beds and tilted layers (Cores 2 and 3 in Fig. 5). This area is interpreted as dominated by redeposition processes and sediment bypassing, particularly during the winter monsoon. Additionally, it is probably the area with the lowest sediment accumulation rate in the subaqueous Mekong delta. This region is also a transition between two regions of a spacious subaqueous delta platform.

Broad topsets with two channels and steep foresets prevail in Area 3 (Fig. 2). This part of the subaqueous Mekong delta is characterised by a high sediment accumulation rate as proved by common horizontal lamination of the sediments (Fig. 5) as well as estimated accumulation rate of >1 cm/yr (core 5, Table 1). The sediments are generally finer than in Area 2. However, their distribution is partly governed by sand deposits on the ridges between the channels and on their flanks while mud occur in the channel troughs (transect 3, Fig. 4). The genesis and formation processes of the channels are not clear. However, tidal ellipses and resulting tidal currents run shoreparallel in that region (Zu et al., 2008). In combination with strong wind-induced shore parallel currents during the winter monsoon season it can lead to higher shear stress near the seabed and increasing erosional condition. Seismic profiles provided by Xue et al. (2010) show erosional pattern in the channel region.

Both areas serve, however, as sedimentary conveyors between Areas 1 and 4. The latter is dominated by the combination of high sediment delivery (SARs >1.4–10 cm/yr (Table 1, Fig. 6)) due to alongshore currents in that region and prevailing low hydrodynamic forces that provide sediment to this depocenter distant from a main river mouth like the Bassac. The presence of predominantly sandy silt and silt also gives the evidence of a low energetic environment supported by laminations with no bioturbation traces (cores 7 and 8, Fig. 5).

Similar sedimentation conditions were found for the most distal region (Area 5) indicated also by very high sediment accumulation rates (>10 cm/yr, Table 1) and finer deposits (about 90% of silt and clay) with no bioturbation traces in X-radiograph negatives (core 9, Fig. 5). However, this region is far from another sediment source and no strong alongshore currents occur that can explain the high sediment accumulation rates.

Borehole data in the lower delta plain indicate facies changes around 3000 cal yr BP (Ta et al., 2002a) due to a shift from “tide-dominated” to “wave and tide-dominated” influences. In contrast, the nine short cores along the transect of more than 400 km in the subaqueous Mekong Delta (Fig. 5) show recent lateral

Table 2
Summary of hydrodynamic factors, morphological features, sedimentary properties as well as sediment accumulation rates (SAR) of the subaqueous Mekong delta subareas.

Delta regions (Fig. 2)	Tides	Waves (relative impact)		River influence		Delta shape	Sediment			Sedimentary structures	SAR
Area	Amplitude in [m]	Summer	Winter	Summer	Winter		Grain size	OM [%]	CC [%]		[cm yr-1]
1	2.5–3.8 (semi-diurnal)	Low	High	High	Moderate	Wide topset (>12 km); steep foreset (<0.2°)	Silty sand to sandy silt	1.5–6.8	0.5–1.7	Laminated sand and silt, crossbedding	Unknown
2	2.5–3.8 (semi-diurnal)	Low	High	Low	Low	Narrow topset (<3.5 km); gentle and wavy shaped foreset (<0.12°)	Sandy silt, sand (local)	2.4–8	0.7–7	Laminated sand and mud; partly bioturbated	Unknown
3	2.5–3.8 (semi-diurnal)	Moderate	Moderate	Low	Low	Wide topset (>15 km) including two channels; steep foreset (<0.4°)	Sandy silt, sand (local)	4–10.2	1.4–16.2	Laminated sand and mud	>1
4	1–2.5 (mixed-tide)	Moderate	Low	Low	Low	Wide (>10 km) and very shallow topset; steep foreset (<0.43°)	Sandy silt to silt	8.3–10.8	2.2–7.2	Laminated mud	>1; Seasonal deposition rate >10
5	0.5–1 (diurnal)	Moderate	Low	Low	Low	Narrow (<2 km) topset; gentle foreset (<0.1°)	Silt	8.4–9.6	2.1–3.7	Homogeneous mud; partly laminated	>1; Seasonal deposition rate >10

alongshore facies changes (Figs. 3C, 4 and 5) under the varying influence of tidal amplitudes, annual alongshore currents and wave impact (Nguyen et al., 2000; Tamura et al., 2010; Xue et al., 2012). However, all facies changes occur in the Mekong River Delta. This example should call attention to the difficulty to interpret sediment facies of a Mega-Delta with many local differences in hydrodynamic conditions at the same time.

5.2. Controlling factors

The monsoon climate controls the sedimentation pattern off the Mekong River mouth and affects the sediment and freshwater discharge and the directions of their distribution (Xue et al., 2011). High precipitation during the summer monsoon season leads to flooding events and irregular water discharge. Moreover, the river outflow has water velocities up to 1 m/s (Wolanski et al., 1996), increasing channel and riverbank erosion (Le et al., 2007). Sediment is transported into the sea and temporarily deposited on tidal flats in nearby river mouth areas. Under summer monsoon conditions, the suspended sediment is also transported in the north-eastern direction due to south-easterly winds and the resulting surface currents.

As proven by the previous studies, sand and relict sand areas cover the adjacent continental shelf that otherwise lacks sediment (Anikiev et al., 2004; Jagodziński, 2005; Schimanski and Stattegger, 2005; Kubicki, 2008). The cluster analysis reveals differences in the delta (Clusters 1 and 2) and the shelf sediments (Cluster 3) concerning its spatial grain size distribution (Fig. 3A and B). Consisting of shell fragments, foraminiferas and concretions from late Pleistocene soils, Cluster 3 reflects the presence of the sediment fraction >1 mm that occurs on the shelf area, except along the foresets in the Gan Hao region (Fig. 3C). This fraction increases the carbonate content in surface samples close to the delta base and serves as a good proxy for the delta-shelf transition. Similar sedimentary features in bottomsets are described for the clinoform in the Gulf of Papua (Walsh et al., 2004) and the Atchafalaya Shelf (Neill and Allison, 2005).

Composed mostly of silt and clay, the suspended sediment may be temporarily deposited on the inner shelf and delivered by a suspension plume (Wolanski et al., 1996). The East Asian winter monsoon may cause reworking by wind-induced currents and sediment transport towards the southwest. The mechanism of temporal deposition of the fine-grained sediments on the inner shelf during the high sediment discharge season and the subsequent redeposition to the final depocenter that is usually located farther offshore in the mid-shelf mud belts and clinoforms is commonly reported from various settings (McKee et al., 1983; Crockett and Nittrouer, 2004; Nittrouer et al., 2009; Szczuciński et al., 2009; Walsh and Nittrouer, 2009). However, in the shelf region offshore the Mekong Delta branches prevail sandy sediment (Anikiev et al., 2004; Kubicki, 2008). Cluster 3 with its dominant mode in medium sand occurs close to the delta base and correlates with the shelf sediment (Fig. 3A). Furthermore, shell fragments and residuals of lateritic palaeosoils distributed in junction to the shelf imply reworking of old sediment in that region and less sedimentation. It leads to the hypothesis that most of the Mekong sediment delivered into the subaqueous Delta is also finally deposited there. Xue et al. (2010) support this hypothesis with its estimation of the sediment capture from the subaerial and subaqueous Mekong Delta that is $80\pm18\%$ of the annual sediment discharge, at least over the last 3000 yr. Hence, the sediment transport to the outer shelf is limited. Tidal regime changes are considered to be the major factor controlling the delta development. The tides alternate from semi-diurnal over mixed to diurnal tides between the eastern Mekong River branches and the south-western Cape Ca Mau and adjacent Gulf of Thailand (Wolanski et al., 1996; Nguyen et al., 2000; Le et al., 2007). Moreover, the tidal range decreases from northeast to southwest. Small cotidal amplitudes of predominant tidal constituent were provided in the Gulf of Thailand and around Cape Ca Mau, yielding a decrease in the number of floods and ebbs per day and in the tidal current velocities (Fang et al., 1999; Zu et al., 2008). Such conditions privilege fine sediment deposition and are favourable for delta aggradation and progradation. In addition, the development of very shallow subaquatic delta topsets reduces wave impact over the shallow water area and the coast around Cape Ca Mau. In combination with the high sediment accumulation rates of 1.4 up to 10 cm/yr (Table 1) these factors support a fast accretion of the south-western Mekong Delta into the Gulf of Thailand.

5.3. The subaqueous Mekong Delta in classification schemes

Attempting to classify the character of the subaqueous Mekong Delta reveals its complexity. For instance, Walsh and Nittrouer (2009) suggested a hierarchical decision tree to predict the marine dispersal system at a river mouth using basic oceanographic and morphological characteristics, classifying the Mekong dispersal system as a "subaqueous delta clinoform," as in the case of the Amazon or Fly River. Accounting for the depocenter around Cape Ca Mau allows its classification as a "marine dispersal dominated" regime due to the distance to the next main distributary (more than 200 km) and low tidal range (Table 2).

Classifying the Mekong Delta using typical triangle classification scheme after Galloway (1975) with wave, tide and river dominated end members is even more difficult. Lobe switching relocates the main depocenter like in the case of the Yellow River (Wright et al., 1990; Saito et al., 2001). This may lead to different hydrodynamic condition and changes in the sediment delivery into the coastal ocean can occur. According to the predominant hydrodynamic factor, the deltaic lobe will deposit as river-, tide- or wave-dominated. For example, in the Danube delta the most northern Chilia branch with the highest discharge deposits recently as a river-dominated lobe whereas the southerly Sf. Gheorghe arm builds a wave-dominated lobe due to its stronger wave-exposed region (Bhattacharya and Giosan, 2003).

Similarities without consideration for temporal but spatial variation occur in the Mekong River delta between wave- and tide-dominated regions and between regions of different tidal amplitudes (Table 2). In consideration of seasonal variation (monsoon seasons) of prevailing hydrodynamic factors along a coastline of more than 400 km, the triangle classification scheme cannot be applied for the whole Mega-Delta like the Mekong River delta, but for spatial limited region.

6. Conclusion

The data presented in this paper shows that the subaqueous parts of a large delta are quite complex, especially regarding variations in morphological and sedimentary characteristics (Figs. 2 and 5, Table 2) and can be classified in different scales. Five regions, differed by their shape and sediments, of the studied subaqueous Mekong delta vary greatly in its sediment accumulation rates between 1 and >10 cm/yr (Table 1). The sedimentary patterns and also changes within one area depended on their hydro- and morphodynamical regime (Figs. 3C, 4 and 5).

Nittrouer et al. (1984) described differences of the fine scale stratigraphy for the Changjiang (Yangtze) and the Huang He (Yellow) dispersal system based on the ratio of the mixing rate to accumulation rate due to the distance to the next major river mouth. As a result, the proximal deposits of the Yangtze River are physical stratified muds by a high accumulation rate while the distal deposits of the Huang He consist of homogenous mud due to the higher mixing rate and lower accumulation rate. In the Mekong River dispersal system occur physical stratified deposits proximal to the major river mouth of the Bassac (Fig. 5). However, in the distal region (nearly 200 km apart) around the Ca Mau cape there are also physical stratified layers (Fig. 5) showing very high accumulation rates of at least 2.6 cm/yr (Table 1) and the area progrades with 24 m/yr (Xue et al., 2010)

into the Gulf of Thailand. In between, there occur strong bioturbated sediments (core 2 in Fig. 5) as well as moderate sorted sandy deposits (Figs. 3C, 4 and core 3 in Fig. 5). It implies that in this transition region the ratio of mixing rate to accumulation rate must be changed. The most southerly region (Area 3) belongs to this transition region and has a wide spreaded subaqueous clinoform, physical stratified layers along the delta slope and high accumulation rates of 4 cm/yr (Table 1). However, there is also a shore parallel channel system of more than 120 km (Fig. 2). The channel troughs show erosional signatures (Xue et al., 2010) and represent silty sediments while the channel flanks consisting of well sorted fine sand (transect 3, Fig. 4). We hypothesise, the difference of both is that the region in front of the Bassac River obtains its sediments directly from the major Mekong branches while the Ca Mau cape region receive either reworked deposits from the easterly lying subaqueous Mekong delta or also from the fluvial system as suspended sediment. Tamura et al. (2010) described mud and fine sand seasonal deposits in the tidal flats close to one of the major river mouth, which are reworked during the winter monsoon season due to wave impact and may be transported to the southwest of Cape Ca Mau.

The cluster analysis of surface samples indicates two end members for the subaqueous delta and one for the delta shelf transition (Fig. 3A). In addition, the sediment class bigger than 1 mm including shell fragments and residuals of lateritic soils occurs only on the shelf and in a special region of area 2 (Fig. 3C). Vietnamese shelf sediments in front of the major rivers consist mainly of sand (Anikiev et al., 2004; Kubicki, 2008). It indicates a limited sedimentary exchange between the subaqueous delta and the shelf, and that most of the river delivered sediment is trapped in the subaerial and subaqueous Mekong delta.

The trial to classify a Mega-delta in the ternary river-wave-tide forcing system (after Galloway, 1975) occurs with difficulties due to the spatial changes of the hydrodynamic factors along a coast of more than 400 km. Each of our separated areas (Fig. 2) is influenced by different major hydrodynamic factors dependent on the season.

Human impacts accelerate coastal erosion together with relative sea level rise and delta subsidence, neither of which is reported in recent studies of the subaqueous Mekong Delta. Future investigations will therefore benefit from our results.

Acknowledgements

The work was supported by a research grant from the German Research Foundation (DFG_STA401/) and through the scientific cooperation with the Vietnamese Academy of Science and Technology (VAST) and the Ministry of Science and Technology (MOST), Vietnam. Partners from the Institute of Resources Geography (VAST) in Ho Chi Minh City (Vietnam) provided significant help. Additionally, the authors thank the staff of the Leibniz-Laboratory at the Christian-Albrechts-University in Kiel and of the International Atomic Energy Agency in Monaco for their measurements of ^{210}Pb. The laboratory staffs at the Institute of Geography of Christian-Albrechts-University of Kiel (Germany) are acknowledged for access to the Malvern Particle Analyzer for grain size measurement and the Radiology Department (Prüner Gang) in Kiel for measuring the X-radiographs. We thank the two anonymous reviewers for their constructive and critical comments.

References

Anikiev, V.V., Shumilin, E.N., Dudarev, O.V., Botsul, A.I., Zakharova, P.V., Kolesov, G.M., Sapozhnikov, D.Y., Smith, R., 2004. Spatial variability in the distribution of lithological characteristics and chemical elements in the bottom sediments of the South China Sea near the Mekong and Saigon River Deltas. Geochemistry International 42, 1301–1318.

Bhattacharya, J.P., Giosan, L., 2003. Wave-influenced deltas, geomorphological implications for facies reconstruction. Sedimentology 50, 187–210.

Blott, S.J., Pye, K., 2001. GRADISTAT, a grain size distribution and statistics package for the analysis of unconsolidated sediments. Earth Surface Processes and Landforms 26, 1237–1248.

Crockett, J.S., Nittrouer, C.A., 2004. The sandy inner shelf as a repository for muddy sediment, an example from Northern California. Continental Shelf Research 24, 55–73.

Fang, G., Kwok, Y.-K., Yu, K., Zhu, Y., 1999. Numerical simulation of principal tidal constituents in the South China Sea, Gulf of Tonkin and Gulf of Thailand. Continental Shelf Research 19, 845–869.

Flynn, W.W., 1968. The determination of low levels of polonium-210 in environmental materials. Analytica Chimica Acta 43, 221–227.

Gagliano, S.M., McIntire, W.G., 1968. Reports on the Mekong River Delta, p. 144.

Galloway, W.E., 1975. Process framework for describing the morphologic and stratigraphic evolution of deltaic depositional systems. In: Broussard, M.L. (Ed.), Deltas, Models for Exploration Houston Geological Society, pp. 87–98.

Hanebuth, T.J.J., Proske, U., Saito, Y., Nguyen, V.L., Ta, T.K.O., 2012. Early growth stage of a large delta — Transformation from estuarine-platform to deltaic-progradational conditions (the northeastern Mekong River Delta, Vietnam). Sedimentary Geology 261–262, 108–119.

Heiri, O., Lotter, A.F., Lemcke, G., 2001. Loss on ignition as a method for estimating organic and carbonate content in sediments, reproducibility and comparability of results. Journal of Paleolimnology 25, 101–110.

Hordoir, R., Nguyen, K.D., Polcher, J., 2006. Simulating tropical river plumes, a set of parametrizations based on macroscale data, A test case in the Mekong Delta region. Journal of Geophysical Research 111.

Institute of Strategy and Policy on natural resources and environment (ISPONRE), 2009. Vietnam Assessment Report on Climate Change, p. 127.

Jagodziński, R., 2005. Petrography and geochemistry of surface sediments from Sunda and Vietnamese shelves (South China Sea) (Ph.D thesis, Institute of Geology, Adam Mickiewicz University, Poznan, Poland).

Kubicki, A., 2008. Large and very large subaqueous dunes on the continental shelf off southern Vietnam, South China Sea. Geo-Marine Letters 28, 229–238.

Kummu, M., Varis, O., 2007. Sediment-related impacts due to upstream reservoir trapping, the Lower Mekong River. Geomorphology 85, 275–293.

Kummu, M., Lu, X.X., Wang, J.J., Varis, O., 2010. Basin-wide sediment trapping efficiency of emerging reservoirs along the Mekong. Geomorphology 119, 181–197.

Le, T.V.H., Nguyen, H.N., Wolanski, E., Tran, T.C., Haruyama, S., 2007. The combined impact on the flooding in Vietnam's Mekong River delta of local man-made structures, sea level rise, and dams upstream in the river catchment. Estuarine, Coastal and Shelf Science 71, 110–116.

Leslie, C., Hancock, G.J., 2008. Estimating the date corresponding to the horizon of the first detection of 137Cs and 239 + 240Pu in sediment cores. Journal of Environmental Radioactivity 99, 483–490.

McKee, B.A., Nittrouer, C.A., DeMaster, D.J., 1983. Concepts of sediment deposition and accumulation applied to the continental shelf near the mouth of the Yangtze River. Geology 11, 631–633.

Mekong River Commission, 2005. Overview of the Hydrology of the Mekong Basin, pp. 0–73.

Mekong River Commission, 2009. Adaptation to climate change in the countries of the Lower Mekong Basin, regional synthesis report, p. 112.

Milliman, J.D., Meade, R.H., 1983. World-wide delivery of river sediment to the oceans. Journal of Geology 91, 1–21.

Milliman, J.D., Ren, M.E., 1995. River flux to the sea, impact of human intervention on river systems and adjacent coastal areas. Impact on Coastal Habitation. CRC Press, pp. 57–83.

Mitsuguchi, T., Dang, P.X., Kitagawa, H., Uchida, T., Shibata, Y., 2008. Coral Sr/Ca and Mg/Ca records in Con Dao Island off the Mekong Delta, Assessment of their potential for monitoring ENSO and East Asian monsoon. Global and Planetary Change 63, 341–352.

Neill, C.F., Allison, M.A., 2005. Subaqueous deltaic formation on the Atchafalaya Shelf, Louisiana. Marine Geology 214, 411–430.

Nguyen, V.L., Ta, T.K.O., Tateishi, M., 2000. Late Holocene depositional environments and coastal evolution of the Mekong River Delta, Southern Vietnam. Journal of Asian Earth Sciences 18, 427–439.

Nittrouer, C., DeMaster, D., McKee, B., 1984. Fine-scale stratigraphy in proximal and distal deposits of sediment dispersal systems in the East China Sea. Marine Geology 61, 13–24.

Nittrouer, C., Austin, J.A., Field, M.E., Kravitz, J.H., Syvitski, J.P.M., Wiberg, P.L., 2009. Writing a Rosetta Stone, Insights into Continental-Margin Sedimentary Processes and. Blackwell Publishing Ltd., Strata.

Proske, U., Hanebuth, T.J.J., Gröger, J., Diệm, B.P., 2011. Late Holocene sedimentary and environmental development of the northern Mekong River Delta, Vietnam. Quaternary International 230, 57–66.

Robbins, J.A., Edgington, D.N., 1975. Determination of recent sedimentation rates in Lake Michigan using Pb-210 and Cs-137. Geochimica et Cosmochimica Acta 39, 285–304.

Robbins, J.A., Edgington, D.N., Kemp, A.L.W., 1978. Comparative ^{210}Pb, ^{137}Cs, and pollen geochronologies of sediments from Lakes Ontario and Erie. Quaternary Research 10, 256–278.

Saito, Y., Yang, Z., Hori, K., 2001. The Huanghe (Yellow River) and Changjiang (Yangtze River) deltas, a review on their characteristics, evolution and sediment discharge during the Holocene. Geomorphology 41, 219–231.

Santisteban, J.I., Mediavilla, R., López-Pamo, E., Dabrio, C.J., Zapata, M.B.R., García, M.J.G., Castaño, S., Martínez-Alfaro, P.E., 2004. Loss on ignition, a qualitative or quantitative method for organic matter and carbonate mineral content in sediments? Journal of Paleolimnology 32, 287–299.

Schimanski, A., Stattegger, K., 2005. Deglacial and Holocene evolution of the Vietnam shelf, stratigraphy, sediments and sea-level change. Marine Geology 214, 365–387.

Snidvongs, A., Teng, S.-K., 2006. Global International Waters Assessment Mekong River, GIWA Regional assessment 55, p. 75.
Syvitski, J.P.M., Saito, Y., 2007. Morphodynamics of deltas under the influence of humans. Global and Planetary Change 57, 261–282.
Syvitski, J.P.M., Kettner, A.J., Correggiari, A., Nelson, B.W., 2005. Distributary channels and their impact on sediment dispersal. Marine Geology 222–223, 75–94.
Syvitski, J.P.M., Kettner, A.J., Overeem, I., Hutton, E.W.H., Hannon, M.T., Brakenridge, G.R., Day, J., Vorosmarty, C., Saito, Y., Giosan, L., Nicholls, R.J., 2009. Sinking deltas due to human activities. Nature Geoscience 2, 681–686.
Szczuciński, W., Stattegger, K., Scholten, J., 2009. Modern sediments and sediment accumulation rates on the narrow shelf off central Vietnam, South China Sea. Geo-Marine Letters 29, 47–59.
Ta, T.K.O., Nguyen, V.L., Tateishi, M., Kobayashi, I., Saito, Y., Nakamura, T., 2002a. Sediment facies and Late Holocene progradation of the Mekong River Delta in Bentre Province, southern Vietnam, an example of evolution from a tide-dominated to a tide- and wave-dominated delta. Sedimentary Geology 152, 313–325.
Ta, T.K.O., Nguyen, V.L., Tateishi, M., Kobayashi, I., Tanabe, S., Saito, Y., 2002b. Holocene delta evolution and sediment discharge of the Mekong River, southern Vietnam. Quaternary Science Reviews 21, 1807–1819.
Ta, T.K.O., Nguyen, V.L., Tateishi, M., Kobayashi, I., Saito, Y., 2005. Holocene delta evolution and depositional models of the Mekong River Delta, southern Vietnam. SEPM, pp. 453–466.
Tamura, T., Saito, Y., Sieng, S., Ben, B., Kong, M., Sim, I., Choup, S., Akiba, F., 2009. Initiation of the Mekong River delta at 8 ka, evidence from the sedimentary succession in the Cambodian lowland. Quaternary Science Reviews 28, 327–344.
Tamura, T., Horaguchi, K., Saito, Y., Nguyen, V.L., Tateishi, M., Ta, T.K.O., Nanayama, F., Watanabe, K., 2010. Monsoon-influenced variations in morphology and sediment of a mesotidal beach on the Mekong River delta coast. Geomorphology 116, 11–23.
Tamura, T., Saito, Y., Nguyen, V.L., Ta, T.K.O., Bateman, M.D., Matsumoto, D., Yamashita, S., 2012. Origin and evolution of interdistributary delta plains; insights from Mekong River delta. Geology 40, 303–306.
Vörösmarty, C.J., Meybeck, M., Fekete, B., Sharma, K., Green, P., Syvitski, J.P.M., 2003. Anthropogenic sediment retention, major global impact from registered river impoundments. Global and Planetary Change 39, 169–190.
Walsh, J.P., Nittrouer, C.A., 2009. Understanding fine-grained river-sediment dispersal on continental margins. Marine Geology 263, 34–45.
Walsh, J.P., Nittrouer, C.A., Palinkas, C.M., Ogston, A.S., Sternberg, R.W., Brunskill, G.J., 2004. Clinoform mechanics in the Gulf of Papua, New Guinea. Continental Shelf Research 24, 2487–2510.
Wang, H., Saito, Y., Zhang, Y., Bi, N., Sun, X., Yang, Z., 2011. Recent changes of sediment flux to the western Pacific Ocean from major rivers in East and Southeast Asia. Earth-Science Reviews 108, 80–100.
Wendong, F., Zhongxin, G., Yuting, H., 1998. Observational study of the circulation in the southern South China Sea. Chinese Science Bulletin 43, 898–905.
Wolanski, E., Ngoc Huan, N., Trong Dao, L., Huu Nhan, N., Ngoc Thuy, N., 1996. Fine-sediment dynamics in the Mekong River Estuary, Vietnam. Estuarine, Coastal and Shelf Science 43, 565–582.
Wright, L.D., Wiseman Jr., W.J., Yang, Z.-S., Bornhold, B.D., Keller, G.H., Prior, D.B., Suhayda, J.N., 1990. Processes of marine dispersal and deposition of suspended silts off the modern mouth of the Huanghe (Yellow River). Continental Shelf Research 10, 1–40.
Xue, Z., Liu, J.P., DeMaster, D., Nguyen, V.L., Ta, T.K.O., 2010. Late Holocene evolution of the Mekong Subaqueous Delta, Southern Vietnam. Marine Geology 269, 46–60.
Xue, Z., Liu, J.P., Ge, Q., 2011. Changes in hydrology and sediment delivery of the Mekong River in the last 50 years, connection to damming, monsoon, and ENSO. Earth Surface Processes and Landforms 36, 296–308.
Xue, Z., He, R., Liu, J.P., Warner, J.C., 2012. Modeling transport and deposition of the Mekong River sediment. Continental Shelf Research 37, 66–78.
Yang, S.L., Milliman, J.D., Li, P., Xu, K., 2011. 50,000 dams later: erosion of the Yangtze River and its delta. Global and Planetary Change 75, 14–20.
Zu, T., Gan, J., Erofeeva, S.Y., 2008. Numerical study of the tide and tidal dynamics in the South China Sea. Deep Sea Research Part I: Oceanographic Research Papers 55, 137–154.